Robust Control Parameters Design of PBC Controller for *LCL*-Filtered Grid-Tied Inverter

Jinping Zhao, Weimin Wu, *Member, IEEE*, Zhikang Shuai, *Senior Member, IEEE*, An Luo, *Senior Member, IEEE*, Henry Shu-hung Chung, *Fellow, IEEE*, and Frede Blaabjerg, *Fellow, IEEE*

***Abstract*—Owing to the strong robustness against system parameter changes and external perturbations, the passivity-based control (PBC) has been widely adopted in grid-tied inverter (GTI). However, for a PBC-based GTI with *LCL*-filter, there are three damping gains and two interactively coupled-feedforward terms in the control loop, resulting in the controller design challenge for engineers. In order to help electrical engineers to well design the PBC controller for *LCL*-filtered GTI, a new design of the damping gains is proposed, by limiting the inherent steady-state error of grid-injected current. Furthermore, the state observer is also adopted to reduce the number of sensors. The robustness against the parameters shift and wide grid impedance variation is also addressed. The effectiveness of the proposed control design strategy will be verified through experimental results on a 3 kW/3-phase/110 V experimental lab setup.**

***Index Terms*—Damping gain, grid-tied inverter, *LCL* filter, passivity-based control, steady-state error.**

I. Introduction

In RECENT years, the development of renewable energy has received significant attention. In renewable generation systems, voltage source grid-tied inverter (GTI) is a key device for linking the power generation equipment to the power grid [1]. In order to satisfy the harmonic standards of grid-injected current, generally, the output filter of GTI has to be adopted, where the *LCL* filter is utilized in most situations, owing to its good performance in the harmonic attenuation and low cost of metallic devices [2]. However, the *LCL* filter may cause possible resonance and great difficulty in the controller design of GTI, due to parameters shift as well as wide equivalent grid impedance variation [3].

Many conventional linear control methods, such as proportional-integral (PI) and proportional-resonant (PR) with passive [4]–[6], active [7]–[11], or hybrid [12]–[14] damping techniques, had been widely studied to suppress the possible resonance. Although these mentioned control methods can achieve stability under the condition of wide grid impendence variation, many shortcomings still exist. For instance, the passive damping method will lead to extra damping power losses, while the active damping (AD) method like the capacitor current feedback (CCF) will increase the number of sensors and the extra measure should be taken [3], [7], [8]. What is more, if the characteristic resonant frequency (f_r) of the *LCL*-based system using conventional CCF AD control method is equal to 1/6 of the sampling frequency (f_s), the digitally controlled GTI with the total delay of $1.5/f_s$ ($1/f_s$ for sampling delay and $0.5/f_s$ for PWM delay) can be hardly stable [15]. Although this problem can be solved by capacitor current PI positive feedback, more sensors should be utilized [8]. In other words, the parameters shift of the *LCL* filter should be limited in a reasonable range for the CCF AD control-based GTI, if no extra measure is taken.

Due to the above shortcomings in conventional control method, a series of nonlinear control methods, which may provide a better solution for an essential nonlinear system such as GTI, have been also studied more and more frequently, including the adaptive control [16]–[19], the deadbeat control [20]–[22], the model predictive control [23]–[26], the slide model control [27], [28], and the passivity-based control (PBC) [30]–[44], etc.

As one of the attractive nonlinear control methods, the PBC is a model-based control method, which contains the energy-shaping and damping-injection [45]. With the merits of clear physical significance, simple modeling process and strong robustness to system parameter changes, the PBC has become a powerful control strategy in power electronics [38], [42], [45]. It also can be seen as a hybrid control scheme, since it includes the instruction predicting feedforward control, the disturbance feedforward control, the decoupling control and the negative feedback control [39]. Currently, the PBC method had been successfully used in the switched reluctance based wind system [30], railway systems [31], [32], the energy storage systems [33], [34], the ac–dc converter [35], the islanded ac microgrid [36] and the GTI systems [37]–[43], etc. In the application of GTI systems, the PBC controllers have different structures with

Manuscript received August 8, 2019; revised November 18, 2019; accepted December 26, 2019. Date of publication December 30, 2019; date of current version April 22, 2020. This work was supported in part by the National Natural Science Foundation of China under Grant 51877130, in part by the National Natural Science Foundation of China under Grant 51561165013, in part by the Shanghai Science and Technology Commission under Grant 17040501500, and in part by the National Key Research and Development Project of China under Grant 2017YFGH001164. Recommended for publication by Associate Editor L. Peng. *(Corresponding author: Weimin Wu.)*

J. Zhao and W. Wu are with the Electrical Engineering Department, Shanghai Maritime University, Shanghai 201306, China (e-mail: zhaojinpingzjp@gmail.com; wmwu@shmtu.edu.cn).

Z. Shuai and A. Luo are with the College of Electrical and Information Engineering, Hunan University, Changsha 410082, China (e-mail: zhikangshuai@hotmail.com; an_luo@126.com).

H. S.-hung Chung is with the Department of Electrical Engineering and the Centre for Smart Energy Conversion and Utilization Research, City University of Hong Kong, Hong Kong (e-mail: eeshc@cityu.edu.hk).

F. Blaabjerg is with the Energy Engineering Department, Aalborg University, 9100 Aalborg, Denmark (e-mail: fbl@et.aau.dk).

Color versions of one or more of the figures in this article are available online at http://ieeexplore.ieee.org.

Digital Object Identifier 10.1109/TPEL.2019.2963200

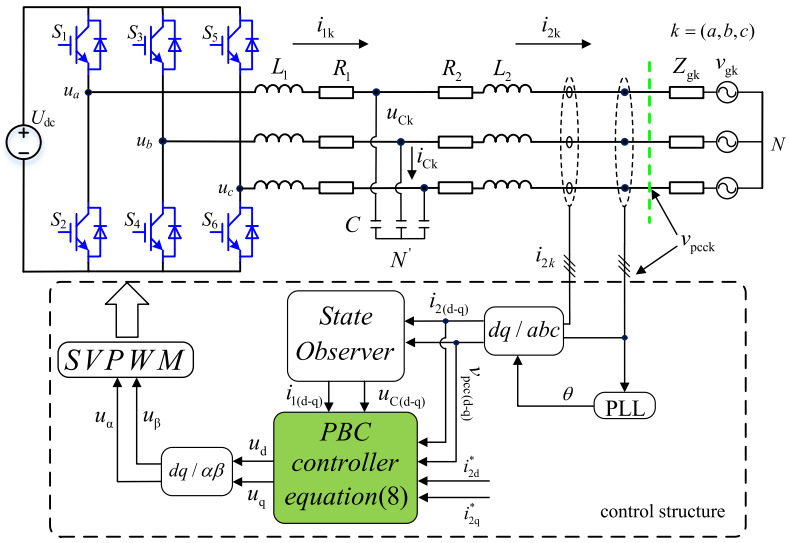

Fig. 1. Control diagram of *LCL*-filtered GTI using the PBC controller.

different power filters, such as *L* filter-based systems [37]–[39], *LC* filter-based systems [40]–[42], and *LCL* filter-based system [43], [44]. Whatever, it is no doubt that the control parameters, named as the damping gains in the PBC controller, are a very important factor during the design.

In [39], the damping gain in the PBC controller was well designed through discrete root locus and unit step response, where the upper limit of damping gain was obtained through discrete root locus and then the suitable value was selected via unit step response. In [40], the damping gain was determined by the traditional analysis method, which is similar to the design of the proportional coefficient for a PI controller. In [41] and [42] the damping gain was selected through attenuating the delay influence on the inverter to realize a passive system. Note that in [39]–[42], there is only one PBC control loop exists. Therefore, during designing this damping gain, the effect of feedforward term can be neglected since it has no effect on system stability.

However, different from the objects in [39]–[42], the PBC-based *LCL*-filtered GTI system need three state variables to participate in the calculation, thus there are three damping gains and two interactively coupled-feedforward terms in the control loop, which are shown in Fig. 2 with different colors. In this case, the conventional design methods using opened-loop design method as introduced in [39]–[42] are not available, since the feedforward terms cannot be directly neglected anymore, resulting in the controller design challenge for engineers. Although in [43], the PBC controller is designed for the *LCL*-filtered system, however, how to choose the damping gains had not been addressed. In [44], the damping gains design was introduced, nevertheless, the delay issue limiting the control bandwidth was ignored.

In order to help electrical engineers to well design the PBC controller for *LCL*-filtered GTI, a new step-by-step control parameters design strategy, which is based on the constraint condition of limiting the inherent steady-state error of grid-injected current, is proposed in this article. Furthermore, in order to reduce the number of sensors as well as costs, the state observer [46], [47] is also adopted in the proposed PBC controller. At the same time, an additional integral regulator is finally adopted to achieve zero steady-state error of grid-injected current.

The rest of this article is organized as follows. The mathematical model and the deduction of PBC control law of *LCL*-filtered GTI are first introduced in Section II. Then, the design of three damping gains by limiting the inherent steady-state error of grid-injected current is proposed in Section III-A brief introduction for the state observer and method to achieve the zero steady-state error of grid-injected current are presented in Section IV. Next, a 3 kW/3-phase/110 V experimental device is constructed with dSPACE DS1202 to verify the effectiveness of the proposed control parameters design strategy in Section V. Finally, there is a conclusion in Section VI.

II. Mathematical Model and PBC Control Law Deduction of *LCL*-Filtered Grid-Tied Inverter

A. Mathematical Model

The topological structure diagram of *LCL*-filtered GTI using the PBC controller is shown in Fig. 1. The *LCL* filter is represented by L_1, C, and L_2, where R_1 and R_2 represent the line resistances and parasitic resistances of L_1 and L_2, respectively. The grid-injected current is represented by i_{2k} ($k = a, b, c$), which is sensed for the overcurrent protection and closed-loop feedback control. v_{pcck} ($k = a, b, c$) represents the voltage of point of common coupling, which is sensed for the synchronization and input of the PBC controller. u_k, i_{1k} and i_{Ck} ($k = a, b, c$) are the inverter side voltage and current and capacitor current, respectively. v_{gk} ($k = a, b, c$) and Z_g denote the ideal grid voltage and the equivalent grid impedance, respectively. Z_g is complex impedance with the inductance of L_g and the resistance of R_g. The dc bus voltage is denoted by U_{dc}. The control structure is given in the dash frame as shown in Fig. 1, where the sampling, the transformation, and the control process are illustrated, and the space vector pulsewidth modulation (PWM) technology is employed to obtain the driving signals.

Similar as introduced in [43], the mathematical model of the *LCL*-filtered GTI can be deduced by applying the Kirchhoff voltage and current laws. And then we obtain

$$\begin{cases} L_1\dfrac{di_{1\mathrm{k}}}{dt}+R_1 i_{1\mathrm{k}}+u_{\mathrm{Ck}}=u_k \\ C\dfrac{du_{\mathrm{Ck}}}{dt}+i_{2\mathrm{k}}-i_{1\mathrm{k}}=0 \\ L_2\dfrac{di_{2\mathrm{k}}}{dt}+R_2 i_{2\mathrm{k}}-u_{\mathrm{Ck}}=-v_{\mathrm{pcck}} \end{cases}, \quad (k=a,b,c). \tag{1}$$

In order to get a better control performance, the *a–b–c* to *d–q* transformation is applied to (1), and the new equations in *d–q* coordinates can be described as follows:

$$\begin{cases} L_1\dfrac{di_{1\mathrm{d}}}{dt}+R_1 i_{1\mathrm{d}}-\omega L_1 i_{1\mathrm{q}}+u_{\mathrm{Cd}}=u_d \\ L_1\dfrac{di_{1\mathrm{q}}}{dt}+R_1 i_{1\mathrm{q}}+\omega L_1 i_{1\mathrm{d}}+u_{\mathrm{Cq}}=u_q \end{cases}$$

$$\begin{cases} C\dfrac{du_{\mathrm{Cd}}}{dt}+i_{2\mathrm{d}}-\omega C u_{\mathrm{Cq}}-i_{1\mathrm{d}}=0 \\ C\dfrac{du_{\mathrm{Cq}}}{dt}+i_{2\mathrm{q}}+\omega C u_{\mathrm{Cd}}-i_{1\mathrm{q}}=0 \end{cases}$$

$$\begin{cases} L_2\dfrac{di_{2\mathrm{d}}}{dt}+R_2 i_{2\mathrm{d}}-\omega L_2 i_{2\mathrm{q}}-u_{\mathrm{Cd}}=-v_{\mathrm{pccd}} \\ L_2\dfrac{di_{2\mathrm{q}}}{dt}+R_2 i_{2\mathrm{q}}+\omega L_2 i_{2\mathrm{d}}-u_{\mathrm{Cq}}=-v_{\mathrm{pccq}} \end{cases}. \tag{2}$$

To simplify analysis and stability judgments, the Euler Lagrange (EL) model is adopted to describe the whole system. Define state variables as $x=(\,i_{1\mathrm{d}}\ i_{1\mathrm{q}}\ u_{\mathrm{Cd}}\ u_{\mathrm{Cq}}\ i_{2\mathrm{d}}\ i_{2\mathrm{q}}\,)^T$, then (2) can be rewritten in the EL form as follows:

$$M\dot{x}+Jx+Rx=u \tag{3}$$

where

$$M=\begin{pmatrix} L_1 & 0 & 0 & 0 & 0 & 0 \\ 0 & L_1 & 0 & 0 & 0 & 0 \\ 0 & 0 & C & 0 & 0 & 0 \\ 0 & 0 & 0 & C & 0 & 0 \\ 0 & 0 & 0 & 0 & L_2 & 0 \\ 0 & 0 & 0 & 0 & 0 & L_2 \end{pmatrix},$$

$$J=\begin{pmatrix} 0 & -\omega L_1 & 1 & 0 & 0 & 0 \\ \omega L_1 & 0 & 0 & 1 & 0 & 0 \\ -1 & 0 & 0 & -\omega C & 1 & 0 \\ 0 & -1 & \omega C & 0 & 0 & 1 \\ 0 & 0 & -1 & 0 & 0 & -\omega L_2 \\ 0 & 0 & 0 & -1 & \omega L_2 & 0 \end{pmatrix},$$

$$R=\begin{pmatrix} R_1 & 0 & 0 & 0 & 0 & 0 \\ 0 & R_1 & 0 & 0 & 0 & 0 \\ 0 & 0 & 0 & 0 & 0 & 0 \\ 0 & 0 & 0 & 0 & 0 & 0 \\ 0 & 0 & 0 & 0 & R_2 & 0 \\ 0 & 0 & 0 & 0 & 0 & R_2 \end{pmatrix},$$

and $u=(\,u_d\ u_q\ 0\ 0\ -v_{\mathrm{pccd}}\ -v_{\mathrm{pccq}})^T$.

According to the passivity theory, the *LCL*-filtered system is strictly passive as introduced in [43]. Therefore, the PBC can be applied to design the controller [45].

B. PBC Control Law Deduction

Define the reference state variables as follows:

$$x^*=\left(\,i_{1\mathrm{d}}^*\ i_{1\mathrm{q}}^*\ u_{\mathrm{Cd}}^*\ u_{\mathrm{Cq}}^*\ i_{2\mathrm{d}}^*\ i_{2\mathrm{q}}^*\,\right)^T. \tag{4}$$

If the error vector is defined as $x_{\mathrm{e}}=x^*-x$, then an error EL equation can be obtained as follows:

$$\begin{aligned} &M\left(\dot{x}^*-\dot{x}_e\right)+J(x^*-x_e)+R\left(x^*-x_e\right)=u \\ &M\dot{x}_e+Jx_e+Rx_e=M\dot{x}^*+Jx^*+Rx^*-u. \end{aligned} \tag{5}$$

In order to accelerate the speed of the convergence, a damping matrix R_{d} can be added to the error system. Then, the injection damping matrix and new dissipation matrix are obtained as follows:

$$\begin{aligned} R_d&=\mathrm{diag}\{\,r_3\ r_3\ r_2\ r_2\ r_1\ r_1\,\}, \\ R_{\mathrm{new}}&=R+R_d \end{aligned} \tag{6}$$

where r_1, r_2, $r_3>0$. Substitution (6) into (5), the new error equation can be obtained as follows:

$$M\dot{x}_e+Jx_e+R_{\mathrm{new}}x_e=M\dot{x}^*+Jx^*+Rx^*+R_dx_e-u. \tag{7}$$

According to (7), if x_{e} equals to zero, the left-hand side of (7) also equals to zero. Then, expand (7), and the control law can be described in detail as follows:

$$\begin{cases} L_1\dfrac{di_{1\mathrm{d}}^*}{dt}+R_1 i_{1\mathrm{d}}^*-\omega L_1 i_{1\mathrm{q}}^*+r_3\left(i_{1\mathrm{d}}^*-i_{1\mathrm{d}}\right)+u_{\mathrm{Cd}}^*=u_d \\ L_1\dfrac{di_{1\mathrm{q}}^*}{dt}+R_1 i_{1\mathrm{q}}^*+\omega L_1 i_{1\mathrm{d}}^*+r_3\left(i_{1\mathrm{q}}^*-i_{1\mathrm{q}}\right)+u_{\mathrm{Cq}}^*=u_q \end{cases}$$

$$\begin{cases} C\dfrac{du_{\mathrm{Cd}}^*}{dt}-\omega C u_{\mathrm{Cq}}^*+r_2(u_{\mathrm{Cd}}^*-u_{\mathrm{Cd}})+i_{2\mathrm{d}}^*-i_{1\mathrm{d}}^*=0 \\ C\dfrac{du_{\mathrm{Cq}}^*}{dt}+\omega C u_{\mathrm{Cd}}^*+r_2(u_{\mathrm{Cq}}^*-u_{\mathrm{Cq}})+i_{2\mathrm{q}}^*-i_{1\mathrm{q}}^*=0 \end{cases}$$

$$\begin{cases} L_2\dfrac{di_{2\mathrm{d}}^*}{dt}+R_2 i_{2\mathrm{d}}^*-\omega L_2 i_{2\mathrm{q}}^*+r_1(i_{2\mathrm{d}}^*-i_{2\mathrm{d}})-u_{\mathrm{Cd}}^*=-v_{\mathrm{pccd}} \\ L_2\dfrac{di_{2\mathrm{q}}^*}{dt}+R_2 i_{2\mathrm{q}}^*+\omega L_2 i_{2\mathrm{d}}^*+r_1(i_{2\mathrm{q}}^*-i_{2\mathrm{q}})-u_{\mathrm{Cq}}^*=-v_{\mathrm{pccq}} \end{cases}. \tag{8}$$

According to (8), the equivalent system diagram of *LCL*-filtered GTI using the PBC controller in the Laplace domain is plotted in Fig. 2.

As shown in Fig. 2, the parameters in the controller are marked with subscript "e" to distinguish control parameters and actual parameters. For example, s$L_{1\mathrm{e}}$ and $R_{1\mathrm{e}}$ are control parameters, while sL_1 and R_1 are actual parameters in the physical object. Due to the symmetrical structure, only the *d*-axis is drawn here, where $e^{-1.5sTs}$ represents the calculation and PWM delay which almost selected as 1.5 T_{s} (T_{s} is the switching or sampling cycle). Note that in order to further analyze the effect caused by the equivalent grid-impedance, the total inductance in the grid side

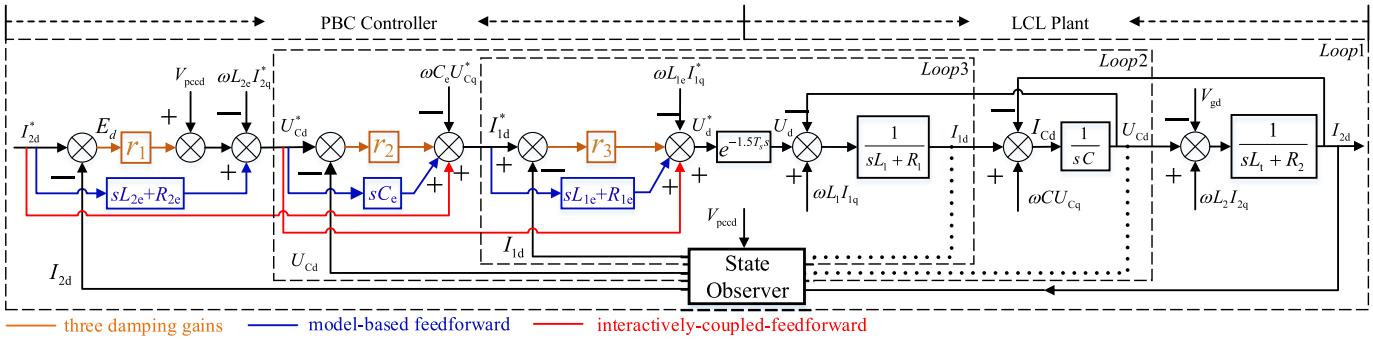

Fig. 2. Equivalent system diagram of *LCL*-filtered GTI using the PBC controller with state observer.

is represented as $L_{\rm t}$ ($L_2 + L_{\rm g}$), while the equivalent resistor of $L_{\rm t}$ is still converted into R_2.

C. Design Challenge of Damping Gains

From Fig. 2, it can be found that due to the using of three state variables (i_1, $U_{\rm C}$, i_2), there are two interactively coupled-feedforward terms marked in red, three model-based feedforward terms marked in blue, and three damping gains terms (r_1, r_2, r_3) marked in brown. Therefore, the whole controller is a complex multiloop controller.

According to the traditional control theory, a double-loop controller can be well designed, based on the relationship of control bandwidth between the inner loop and the outer one [49]. The similar method is adopted for a three-loop controller [50]. It should be pointed out that the GTI with the classic three-loop controller has poor dynamic performance under the weak grid condition in theory, especially when the switching frequency is not so high. Furthermore, as shown in Fig. 2, there are two interactively coupled-feedforward terms between the three control loops, and every loop is coupled connected with the interactively coupled-feedforward terms in red. Therefore, there is a strong coupling relationship between these control loops, resulting in more design difficulty with the traditional three-loop design theory as introduced in [50].

Generally, the trial and error method is often adapted to design control parameters in a nonlinear system, but at the cost of computing resources, especially when there is no suitable guidance. Furthermore, it is also difficult to use the intelligent optimization algorithm to design these three damping gains, because the optimization cost function is difficult to be defined for this system, and there is not enough tangible constrains.

Therefore, it is very valuable to introduce a practical parameters design strategy for *LCL*-filtered GTI using the PBC controller, which does help for the industrial applications. Note that in theory, more sensors should be adopted to obtain the state variables of the PBC controller, resulting in extra sensing costs. In this article, a separated loop control parameters design strategy will be proposed, and the state observer technology will be also utilized to reduce the number of sensors. The detailed description will be given in the next two sections.

III. Proposed Design of Damping Gains by Limiting the Inherent Steady-State Error of Grid-Injected Current

As shown in Fig. 2, the control system can be divided into three control loops from the inner to the outer, which are named as loop3, loop2, and loop1, respectively. First, through the analysis for the inherent steady-state error of grid-injected current, the relationship of three damping gains can be roughly determined. Then, an efficient trial and error procedure can be obtained by using the stability criterion. Finally, due to the stable margin considered in the design procedure, robustness can be easily obtained.

A. Analysis on the Inherent Steady-State Error of Grid-Injected Current

From Fig. 2, it can be seen that the PBC-based GTI is a multi-input multioutput system, when the coupling path between *d*- and *q*- axis is considered. In order to analyze the performance of the PBC controller, the closed-loop transfer function matrix of the whole system is deduced as follows:

$$\begin{aligned}\begin{bmatrix} I_{2\rm d} \\ I_{2\rm q} \end{bmatrix} &= \begin{bmatrix} G_{\rm ddc1} & G_{\rm dqc1} \\ G_{\rm qdc1} & G_{\rm qqc1} \end{bmatrix} \begin{bmatrix} I^*_{2\rm d} \\ I^*_{2\rm q} \end{bmatrix} \\ &= \begin{bmatrix} \dfrac{AD+BC}{C^2+D^2} & \dfrac{AC-BD}{C^2+D^2} \\ \dfrac{BD-AC}{C^2+D^2} & \dfrac{AD+BC}{C^2+D^2} \end{bmatrix} \begin{bmatrix} I^*_{2\rm d} \\ I^*_{2\rm q} \end{bmatrix}. \end{aligned} \tag{9}$$

The expressions of *A, B, C, D* are in the Appendix. As time $t \to \infty$, then $s \to 0$, in the steady-state, the $G_{\rm ddc1}$ and $G_{\rm dqc1}$ in (9) can be rewritten as follows:

$$\begin{aligned} \lim_{t\to\infty} G_{\rm ddc1}(t) &= \lim_{s\to 0} G_{\rm ddc1}(s) = \frac{MN+PQ}{N^2+Q^2} \\ \lim_{t\to\infty} G_{\rm dqc1}(t) &= \lim_{s\to 0} G_{\rm dqc1}(s) = \frac{MQ-NP}{N^2+Q^2} \end{aligned} \tag{10}$$

where

$$\begin{aligned} M = {} & r_1 r_2 R_{1\rm e} + r_2 r_3 R_{2\rm e} + r_2 R_{1\rm e} R_{2\rm e} - \omega^2 r_1 L_{1\rm e} C_e \\ & - \omega^2 L_{1\rm e} r_2 L_{2\rm e} - \omega^2 r_3 C_e L_{2\rm e} - \omega^2 C_e R_{1\rm e} L_{2\rm e} \\ & - \omega^2 L_{1\rm e} C_e R_{2\rm e} + r_1 r_2 r_3 + r_1 + r_3 + R_{1\rm e} + R_{2\rm e} \end{aligned}$$

$$
\begin{aligned}
N &= r_1r_2R_{1e} + r_2r_3R_2 + r_2R_{1e}R_2 - \omega^2 r_1L_{1e}C_e \\
&\quad - \omega^2 r_2L_{1e}L_2 - \omega^2 r_3CL_2 - \omega^2 CR_1L_2 - \omega^2 L_1CR_2 \\
&\quad + r_1r_2r_3 + r_1 + r_3 + R_1 + R_2 \\
P &= \omega r_1C_eR_{1e} + \omega r_2R_{1e}L_{2e} + \omega r_2L_{1e}R_{2e} + \omega r_3C_eR_{2e} \\
&\quad + \omega r_1r_2L_{1e} + \omega r_2r_3L_{2e} + \omega r_1r_3C_e + \omega C_eR_{1e}R_{2e} \\
&\quad - \omega^3 L_{1e}C_eL_{2e} + \omega L_{1e} + \omega L_{2e} \\
Q &= \omega r_1C_eR_{1e} + \omega r_2R_{1e}L_2 + \omega r_2L_{1e}R_2 + \omega r_3CR_2 \\
&\quad + \omega r_1r_2L_{1e} + \omega r_2r_3L_2 + \omega r_1r_3C_e \\
&\quad + \omega CR_1R_2 - \omega^3 CL_1L_2 + \omega L_1 + \omega L_2.
\end{aligned}
$$

From (10), it can be known that if and only if $L_1 = L_{1e}$, $R_1 = R_{1e}$, $C = C_e$, $L_2 = L_{2e}$, $R_2 = R_{2e}$, thenG_{ddc1} equals to one and G_{dqc1} equals to zero, which indicates the system can track the reference value with the zero steady-state error. However, it is impracticable in a real physical system, since the parameter drifting always occurs and the line impedance is changing with the time. If neglecting the external disturbances, the inherent steady-state error of grid-injected current will only depend on r_1, r_2, r_3, $L_{1(e)}$, $R_{1(e)}$, $C_{(e)}$, $L_{2(e)}$, and $R_{2(e)}$. Since r_1, r_2, and r_3 are the damping gains can be artificially tuned, the inherent steady-state error can be controlled within a certain range. Note that the order of magnitude of capacitor (10^{-6}) and inductor (10^{-3}) is very small, many terms related to them, such as the product of $\omega^3 L_{1e}C_eL_{2e}$, can be neglected. Furthermore, the equivalent resistance of inductor is also very small, if a very small value of r_2 is selected (suggest at least 100 times smaller than r_1 and r_3), many terms related to r_2, such as the products of $r_1r_2R_{1e}$,$r_2r_3R_{2e}$, and $r_2R_{1e}R_2$, can be also neglected. And then the percentage of inherent steady-state error of grid-injected current can be simplified as follows:

$$
e\% \approx \frac{R_1 - R_{1e} + R_2 - R_{2e}}{r_1r_2r_3 + r_1 + r_3 + R_1 + R_2} \times 100\%. \tag{11}
$$

From (11), it can be obtained that the larger values of r_1, r_3, the smaller inherent steady-state error. Note that the outer loop damping gain of r_1, which determines the control bandwidth, had better be set as large as possible.

B. Step-by-Step Design of Damping Gains

As described in (9), the transfer function matrix is very complex, which causes trouble to select the control parameters and analyze the system stability. If the coupling path between *d*- and *q*- axis is not addressed, the situation will become much simpler. Note that, as introduced in [50], the coupling terms between *d*- and *q*- axis only have little effect on system stability, and they can be neglected during the controller design. Furthermore, in order to simplify the calculation, the resistances in the controller and physical device are neglected, due to their small values. Based on Fig. 2, the closed-loop transfer function (neglecting coupling terms between *d*- and *q*- axis) of the whole system can be obtained as (12) shown at the bottom of this page.

The PWM and sampling delay term of $e^{-1.5T_s s}$ is approximated as $1/(1.5sT_s + 1)$ [38]. According to the Routh stability criterion, the system will be stable, if $f_1(r_1, r_2, r_3)$ and$f_2(r_1, r_2, r_3)$ are greater than zero, which is described as (13) shown at the bottom of this page.

Based on the analysis of the inherent steady-state error and the Routh stability criterion, the separated loop design strategy of the PBC controller for *LCL*-filtered GTI is proposed, where the detailed design procedure is illustrated in Fig. 3.

Some constraints are defined beforehand as follows.

1) The *LCL* filter is designed according to the current ripple, the rated power, and the IEEE harmonic standard [2].
2) The damping gain r_2 should be 100 times smaller than r_1 and r_3 at least.
3) The settling time of the nested inner loop should be at least 4 times faster than the related outer loop.
4) The overshoot of every closed-loop should be no more than 30% during the unit step response.

Before the control parameters design, the values of the *LCL* filter must be selected, where the filter design criteria can be found in [2], [48]. In our case, a 3 kW/3-phase/110 V experimental setup with the sampling frequency of 10 kHz

$$
G_{c1}(s) = \frac{I_{2d}(s)}{I_{2d}^*(s)} = \frac{\begin{array}{l} s^3C_eL_{1e}L_{2e} + s^2(r_2L_{1e}L_{2e} + r_3C_eL_{2e} + r_1CL_{1e}) \\ + s(r_2r_3L_{2e} + r_1r_2L_{1e} + r_1r_3C_e + L_{1e} + L_{2e}) + r_1r_2r_3 + r_1 + r_3 \end{array}}{\begin{array}{l} s^4 1.5T_sCL_1L_t + s^3CL_1L_t \\ + s^2(r_1C_eL_{1e} + r_3CL_t + L_{1e}r_2L_2 + 1.5T_sL_1 + 1.5T_sL_t) \\ + s(r_1r_2L_{1e} + r_1r_3C_e + r_2r_3L_2 + L_1 + L_t) + r_1r_2r_3 + r_1 + r_3 \end{array}} \tag{12}
$$

$$
f_1(r_1,r_2,r_3) = \frac{r_1C_eL_{1e}}{1.5T_sCL_1L_t} + \frac{r_3}{1.5T_sL_1} + \frac{r_2L_{1e}}{1.5T_sCL_1} - \frac{r_1r_2L_{1e}}{CL_1L_t} - \frac{r_1r_3C_e}{CL_1L_t} - \frac{r_2r_3}{CL_1} \tag{13a}
$$

$$
\begin{aligned}
f_2(r_1,r_2,r_3) &= \frac{r_1r_2L_{1e}}{CL_1L_t} + \frac{r_1r_3C_e}{CL_1L_t} + \frac{r_2r_3}{CL_1} + \frac{1}{CL_t} + \frac{1}{CL_1} \\
&\quad - \frac{r_1r_2r_3 + r_1 + r_3}{[r_1C_eL_{1e} + r_2L_{1e}L_t + r_3CL_t - 1.5T_s(r_1r_2L_{1e} + r_1r_3C_e + r_2r_3L_t)]}
\end{aligned} \tag{13b}
$$

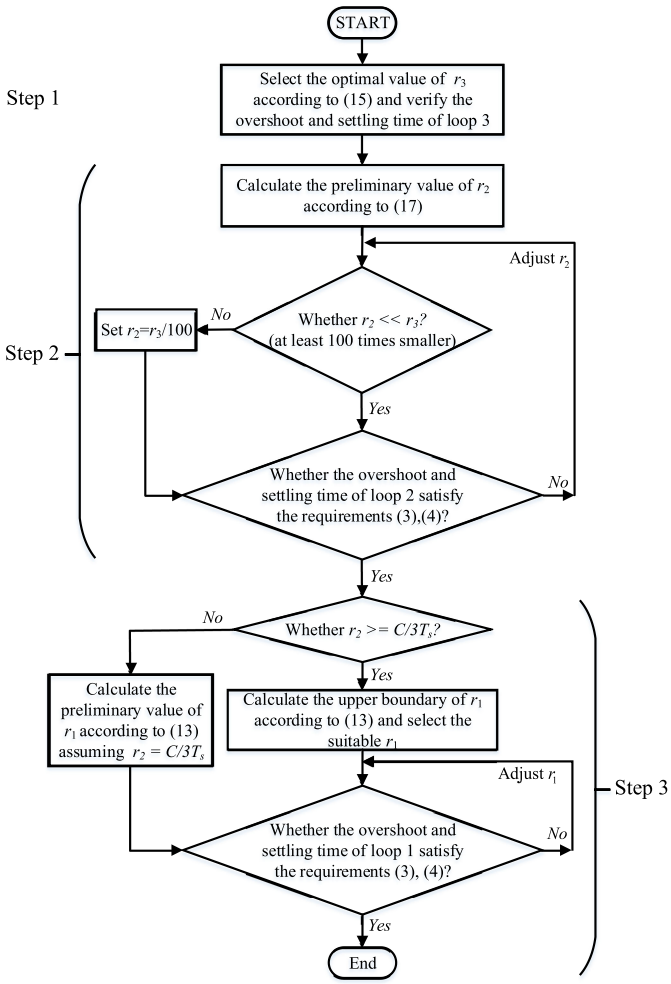

Fig. 3. Proposed design strategy for PBC-based GTI with *LCL*-filter.

is constructed. According to the calculation formula in [2], [48], then L_1, L_2, and C are chosen as 1.2 mH, 1.2 mH, and 6 μF, respectively, where the resonant frequency is about 2654 Hz.

Step 1. Select the Optimal Damping Gain of Loop3 (r_3): For three damping gains, the damping gain of loop3 (r_3) should be first determined, where the closed-loop transfer function of loop3 is as follows:

$$G_{c3}(s) = \frac{I_{1\mathrm{d}}(s)}{I_{1\mathrm{d}}^*(s)} = \frac{sL_{1\mathrm{e}} + r_3}{1.5s^2T_sL_1 + sL_1 + r_3} = \frac{s\frac{L_{1\mathrm{e}}}{1.5T_sL_1} + \frac{r_3}{1.5T_sL_1}}{s^2 + s\frac{1}{1.5T_s} + \frac{r_3}{1.5T_sL_1}}. \quad (14)$$

From (14), it can be seen that the closed-loop transfer function of loop3 is similar to a second-order system when the total time delay is addressed. According to the control theory, when the damping ratio ξ is $\sqrt{2}/2$, the system can achieve the optimal model. Thus, r_3 can be calculated as follows:

$$r_3 = \frac{L_1}{6\xi^2T_s}. \quad (15)$$

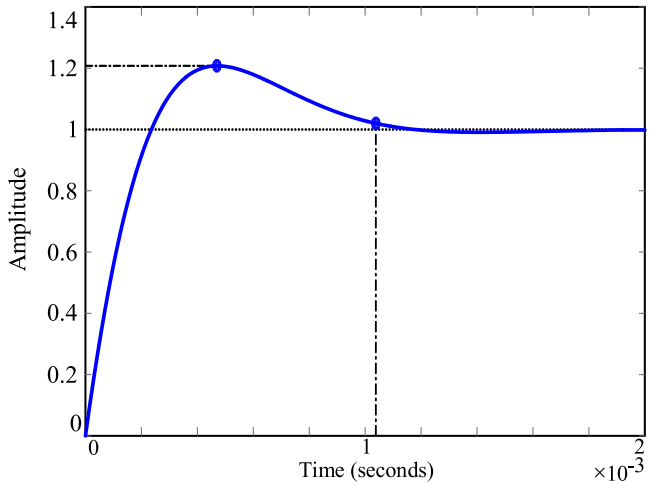

Fig. 4. Unit step response of G_{c3} with $r_3 = 4$.

Taking $L_1 = 1.2$ mH, $\xi = \sqrt{2}/2$, $T_\mathrm{s} = 1/10\,000$ s into (15), $r_3 = 4$ can be obtained in our case. The unit step response of G_{C3} with $r_3 = 4$ is plotted in Fig. 4. Fig. 4 shows that the settling time is about 1.03 ms and the overshoot is about 20%, which indicates that $r_3 = 4$ is the optimal selection.

Step 2. Select the Suitable Damping Gain of Loop2 (r_2): As r_3 is determined, r_2 can be selected next. At the same time, a large sufficient r_1 is expected to satisfy the bandwidth requirement. According to (13), the relationship curves between r_2 and the stable range of r_1 are plotted in Fig. 5, where the *X*-axis represents the value of r_1 which ranges from 0 to 30, and the *Y*-axis represents the calculated result of f_1 and f_2, respectively.

From Fig. 5, it can be seen that the stable range of r_1 is increased as r_2 decreases. Therefore, a larger r_1 can be selected when a smaller r_2 is adopted (suggest at least 100 times smaller than r_1 and r_3), which is consistent with the aim of reducing the inherent steady-state error of grid-injected current. However, if r_2 closes to 0 infinitely, the stable range of r_1 tends to be gigantic. For example, taking $r_2 = 0.01$, the stable range of r_1 is $r_1 \geq 0$. And the precise stable range of r_1 can't be exactly found, due to the approximated expression of the time delay in (13).

Therefore, the critical r_2 is suggested to be defined as the preliminary value, which makes the slope of the line equal to 0 in Fig. 5(a). And it can be obtained via calculating the partial derivation of f_1 in (13a) as follows:

$$\frac{\partial f_1}{\partial r_1} = 0. \quad (16)$$

If the parameters of L_1 and C do not drift, the preliminary value of r_2 can be calculated as follows:

$$r_2 = C/3T_s. \quad (17)$$

It can be found from (17) that the critical value of r_2 is determined by C and T_s. In order to expend the calculable range of r_1, the small C and large T_s are preferred. Taking $C = 6$ μF, $T_\mathrm{s} = 1/10\,000$ s into (17), the preliminary value of r_2 is calculated as 0.02 in our case.

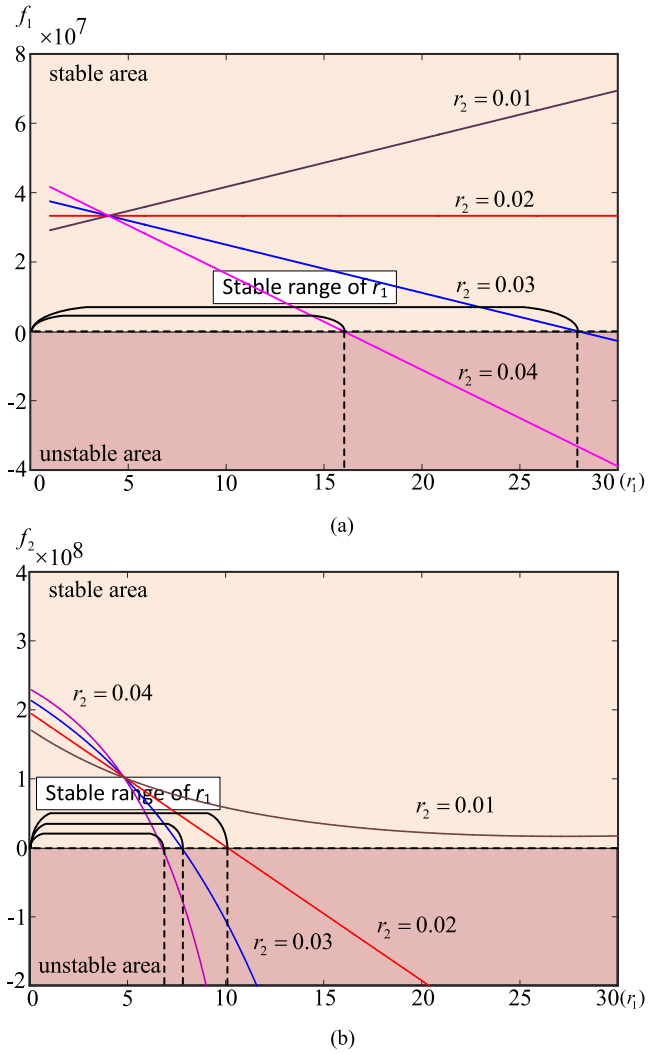

Fig. 5. Stable relationship between r_2 and r_1 according to (13). (a) f_1 and (b) f_2.

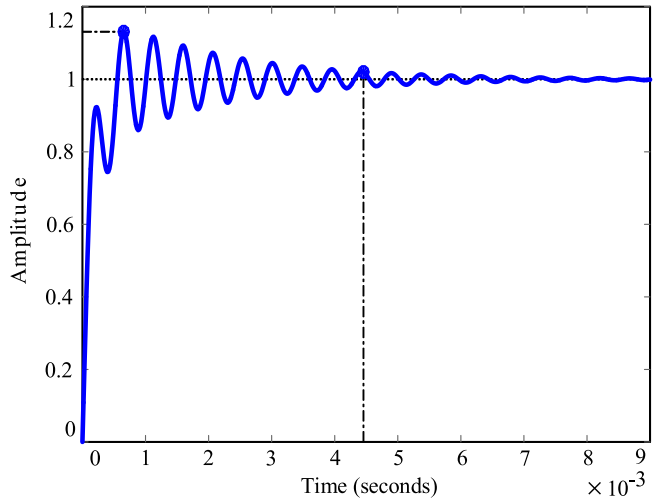

Fig. 6. Unit step response of G_{c2} with $r_3 = 4$, $r_2 = 0.02$.

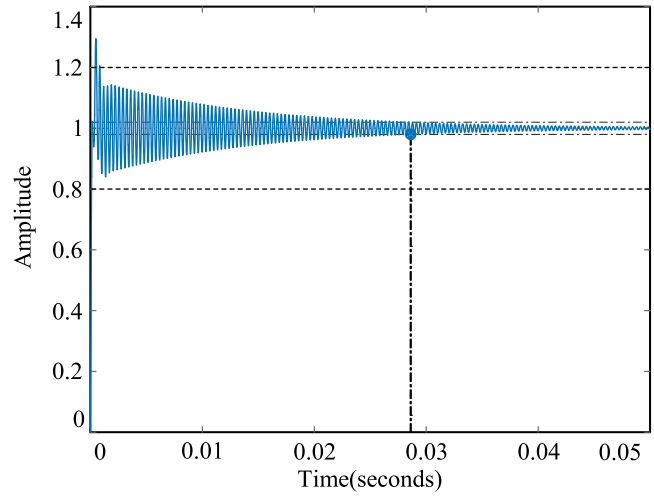

Fig. 7. Unit step response of G_{c1} with $r_1 = 8$, $r_2 = 0.02$, $r_3 = 4$.

In order to analyze the performance of the middle loop and verify requirements of (3) and (4), the closed-loop transfer function of loop2 is deduced as follows:

$$G_{c2}(s) = \frac{U_{\mathrm{Cd}}(s)}{U^*_{\mathrm{Cd}}(s)} = \frac{s^2 L_{1\mathrm{e}} C_e + s r_3 C_e + s L_{1\mathrm{e}} r_2 + r_2 r_3 + 1}{1.5 T_s s^3 C L_1 + s^2 C L_1 + s(1.5 T_s + r_3 C + L_{1\mathrm{e}} r_2) + r_2 r_3 + 1}. \quad (18)$$

Under the condition that $L_{1\mathrm{e}} = L_1$, $C_{\mathrm{e}} = C$, $r_2 = 0.02$, $r_3 = 4$, the unit step response of G_{c2} is plotted in Fig. 6, where the overshoot is less than 20% and the setting time is about 4.46 ms. The requirements of (3) and (4) are both satisfied.

Step 3. Select the Suitable Damping Gain of Loop1(r_1): If r_2 and r_3 have been determined, the stable range of r_1 can be obtained from (13). For instance, when $r_2 = 0.02$, $r_3 = 4$, the stable range of r_1 is greater than 0 according to f_1, while r_1 should be set between 0 and 10.1 according to f_2. If sufficient stable margins are addressed, r_1 had better be smaller than the upper boundary of 10.1 in our case, and $r_1 = 8$ is selected according to requirements of (3) and (4), where the unit step response of loop1 is depicted in Fig. 7.

C. Robustness Analysis

The robustness of a controller is mainly manifested as its ability to suppress the adverse effect caused by the parameters drift of object. Assume that L_1 changes in the range of 0.8–1.6 mH (±33%), the variation of the capacitor is in the range of 4–8 μF (±33%), and the total grid side inductance $L_{\mathrm{t}} = L_2 + L_{\mathrm{g}}$ varies in the range of 0.8–6 mH (−33%–+400%). The closed-loop pole-zero maps in the discrete domain are drawn in Fig. 8 to investigate the robustness of the PBC controller under above situations. The control parameters used in the PBC controller are designed above, where $r_1 = 8$, $r_2 = 0.02$, $r_3 = 4$.

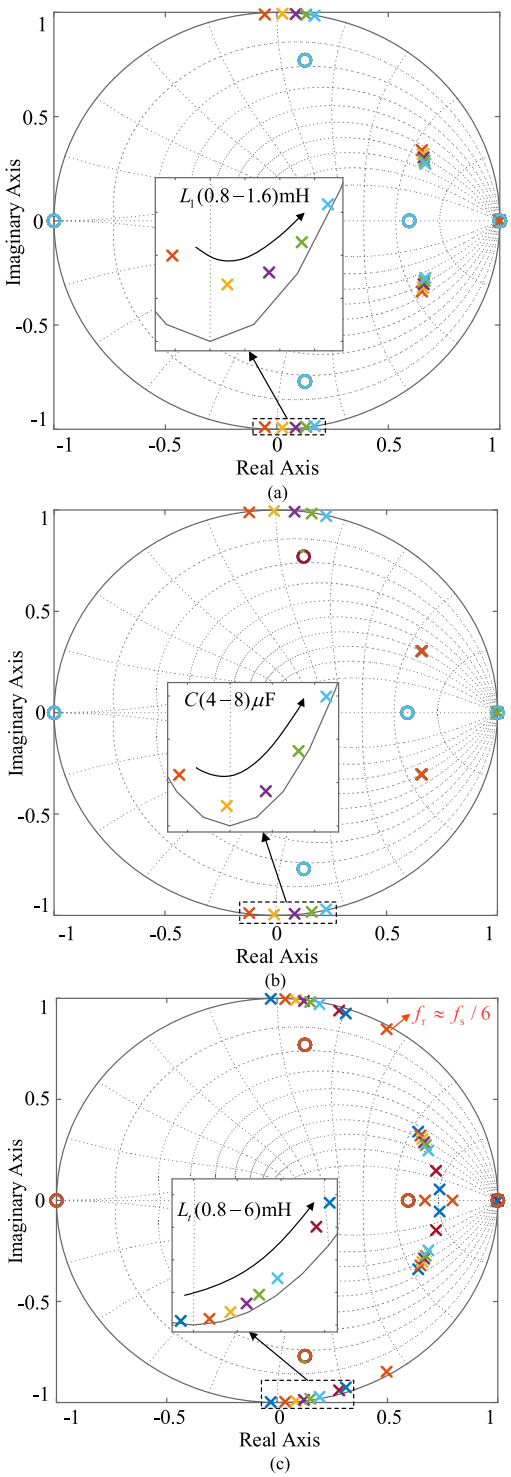

Fig. 8. Closed-loop pole-zero maps of PBC under parameters drift, (a) L_1 drifts, (b) C drifts, (c) L_t drifts and $f_r \approx f_s/6$.

From Fig. 8, it can be seen that all the closed-loop poles are located in the unit circle, which indicates that the system is always stable. Furthermore, as pointed in [15], the *LCL*-filtered GTI system with the conventional CCF AD method can be hardly stable, if $f_r = 1/6\ f_s$ when the total time delay is $1.5/f_s$. Note that Fig. 8(c) proves that when $f_r = 1/6\ f_s$, the proposed PBC controller can still stabilize the system well. Therefore, it can be concluded that compared with the conventional CCF AD method, the proposed PBC has higher robustness against the parameters drift.

IV. State Observer to Save Sensors and Method to Achieve the Zero Steady-State Error

A. State Observer

In order to reduce the number of sensors, the state observer is adopted here, and a brief introduction of state observer is also given.

From (1), the state equation of the system can be rewritten as a matrix form in *d–q* axis

$$\frac{dx'}{dt} = \underbrace{\begin{pmatrix} -\frac{R_1}{L_1} - j\omega & -\frac{1}{L_1} & 0 \\ \frac{1}{C} & -j\omega & -\frac{1}{C} \\ 0 & \frac{1}{L_2} & -\frac{R_2}{L_2} - j\omega \end{pmatrix}}_{A} x' + \underbrace{\begin{pmatrix} \frac{1}{L_1} \\ 0 \\ 0 \end{pmatrix}}_{B_1} u_k + \underbrace{\begin{pmatrix} 0 \\ 0 \\ -\frac{1}{L_2} \end{pmatrix}}_{B_2} v_{\mathrm{pccd-q}},$$

$$x' = \begin{pmatrix} i_{1d-q} \\ u_{\mathrm{Cd-q}} \\ i_{2\mathrm{d-q}} \end{pmatrix}, \quad i_{2\mathrm{d-q}} = \underbrace{\begin{pmatrix} 0 & 0 & 1 \end{pmatrix}}_{C} x'. \tag{19}$$

The state observer is designed with (19), and the needed state variables can be estimated using a full-order observer in practical applications, i.e.

$$\frac{d\hat{x}'}{dt} = A\hat{x}' + B_1 u_k + B_2 v_{\mathrm{pccd-q}} + L(i_{2\mathrm{d-q}} - \hat{i}_{2\mathrm{d-q}}),$$

$$\hat{x}' = \begin{pmatrix} \hat{i}_{1\mathrm{d-q}} \\ \hat{u}_{\mathrm{Cd-q}} \\ \hat{i}_{2\mathrm{d-q}} \end{pmatrix}$$

$$\hat{i}_{2\mathrm{d-q}} = C\hat{x}' \tag{20}$$

where $\hat{x}'$ is the estimated variable, and L is the observer gain vector. Because the $i_{2\mathrm{k}}$ and v_{pcck} are sensed and the converter voltage u_{k} is internally known, so $i_{1\mathrm{k}}$ and u_{Ck} can be obtained according to (20). Based on (19) and (20), the estimation error $x'_e = x' - \hat{x}'$ is calculated as follows:

$$\frac{dx'_e}{dt} = (A - LC)x'_e. \tag{21}$$

If the matrix of (*A-LC*) satisfies the Hurwitz condition, the estimated variables $\hat{x}'$ can converge to x' gradually, where the detailed analysis process can be found in [46] and [47]. Fig. 9

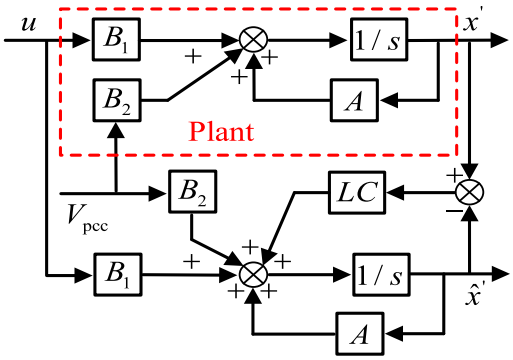

Fig. 9. Block diagram of state observer.

shows the block diagram of the state observer, while its position in the whole system is depicted in Fig. 1.

B. Method to Achieve Zero Steady-State Error

From the above analysis, we know that the PBC method will lead to an inherent steady-state error. And the damping gains can only reduce the value of inherent steady-state error of grid-injected current, but cannot eliminate it. However, the real steady-state error can be easily eliminated by using an additional integral regulator. In recent years, many modified PBC methods to eliminate or reduce the steady-state error had been proposed [38], [40]. In our case, the inherent steady-state error of grid-injected current also can be eliminated by using an additional integral regulator, where the damping gain of r_1 can be replaced by a PI controller with the proportion coefficient of $K_{\rm p} = r_1 = 8$ and the integral coefficient of $K_{\rm i} = 800$ in our case.

V. Experimental Verifications

In this section, the effectiveness of the proposed control parameters design strategy is further studied. The 3 kW/3-phase/110 V GTI experimental lab setup is also developed. The three-phase grid is emulated with a Chroma 61830 three-phase grid simulator, the control algorithm is achieved via dSPACE DS1202 microlabbox, the dc voltage is given by a Chroma 62150H-600S dc power supply, a control desk project is developed to tune control parameters and reference value, and all the waveforms are captured from Yokogawa DL1640 digital oscilloscope. The experimental setup is shown in Fig. 10 and the parameters used for experiments are listed in Table I.

In order to verify the control performance of the PBC controller, many experiments are carried out next. Note that the method to achieve zero steady-state error is not adopted at the beginning. The waveforms in Figs. 11 and 12 are the measured grid-injected currents and their dynamic responses under $L_{\rm g} = 0$ and 4.8 mH, respectively. It can be seen that the grid-injected current is in perfect sinusoidal waveforms with the measured total harmonic distortion (THD) of 1.62% and 2.42%, respectively. Furthermore, in Figs. 11 and 12, the peak values of grid-injected currents are both around 12 A when the references are set as 12. 86 A. Figs. 11 and 12 also show that the response time is less than

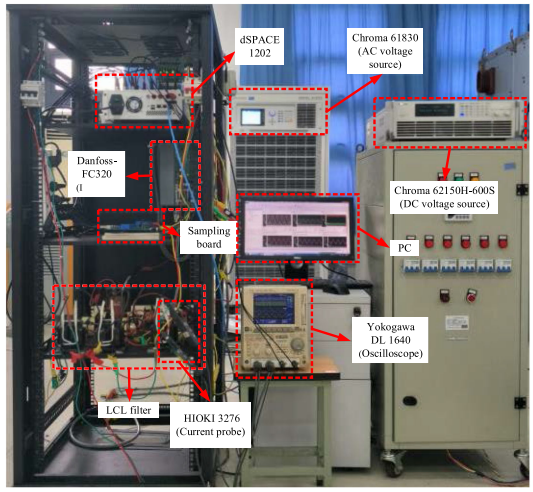

Fig. 10. Experimental device of three-phase *LCL*-filtered GTI.

TABLE I
Simulation and Experiment Parameters for GTI

Symbols	*Description*	*Value*
$V_{\rm g}$	Grid Voltage	110V(RMS)
$f, f_{\rm s}$	Grid ,Switching and sampling frequency	50Hz,10kHz
L_1	Filter side inductor	1.2mH,2mH
C	Filter capacitor	6uF
L_2	Grid side inductor	1.2mH
$L_{\rm g}$	Grid inductance	0mH, 4.8mH
$U_{\rm dc}$	DC bus voltage	350V
$L_{1\rm e}, R_{1\rm e}$	estimated value of L_1 and R_1 in controller	1.2mH, 0.1Ω
$L_{2\rm e}, R_{2\rm e}$	estimated value of L_2 and R_2 in controller	1.2mH, 0.1Ω
r_1, r_2, r_3	Three damping gains	8, 0.02, 4
i_2^*	Reference current	12.86A(peak value)
$K_{\rm p}$	Proportion coefficient	8
$K_{\rm i}$	Integral coefficient	800

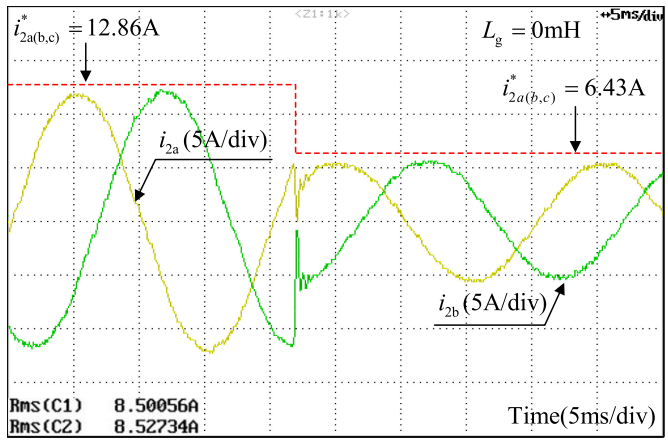

Fig. 11. Measured grid-injected currents and their dynamic responses under $L_{\rm g} = 0$ mH.

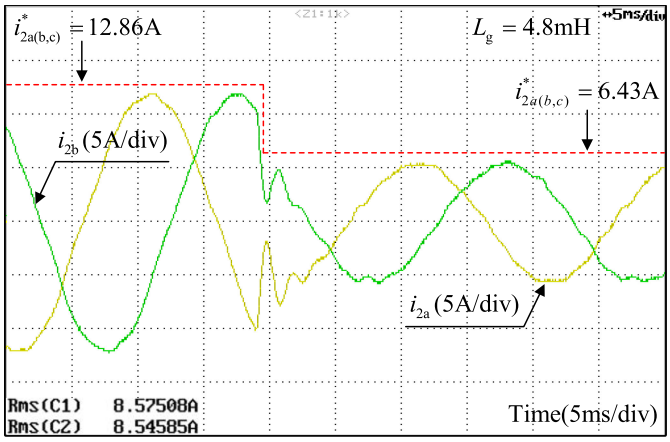

Fig. 12. Measured grid-injected currents and their dynamic responses under $L_g = 4.8$ mH.

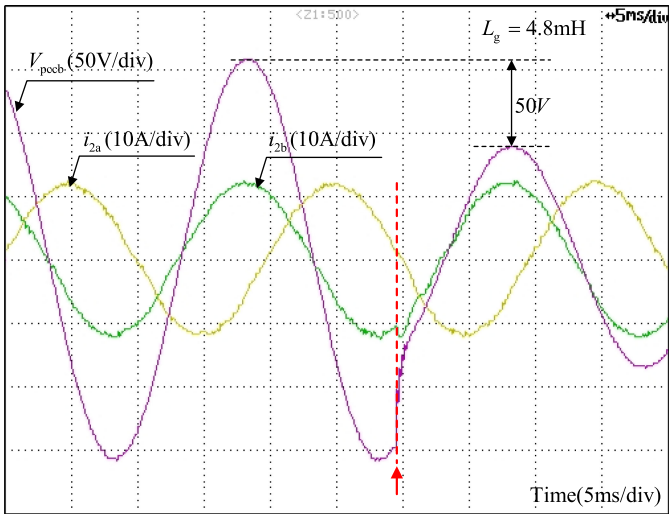

Fig. 13. Grid-injected current under 50 V voltage reduction under $L_g = 4.8$ mH.

a quarter of the cycle. From the data of Figs. 11 and 12, it can be deduced that the proposed PBC control has strong robustness against the wide variation of equivalent grid impedance.

Fig. 13 shows the grid-injected current under the condition of 50 V voltage drop when $L_g = 4.8$ mH, where a very smooth transient process occurs. The dynamic response of grid-injected current under the condition of sharp phase variation when $L_g = 4.8$ mH is depicted in Fig. 14, which also indicates that the dynamic process is fast. All the dynamic results indicate that a satisfactory performance can be successfully achieved with the proposed PBC controller.

The grid voltage background harmonics will affect the quality of the grid-injected current. Fig. 15 shows the measured grid-injected current together with the distorted grid voltage under $L_g = 4.8$ mH. Note that the grid voltage is distorted by the 3rd, 5th, 7th, and 9th harmonic voltages, whose magnitudes with respect to the grid fundamental voltage are all 3%, and the THD of grid-injected current is about 3.37%. It can be seen that the

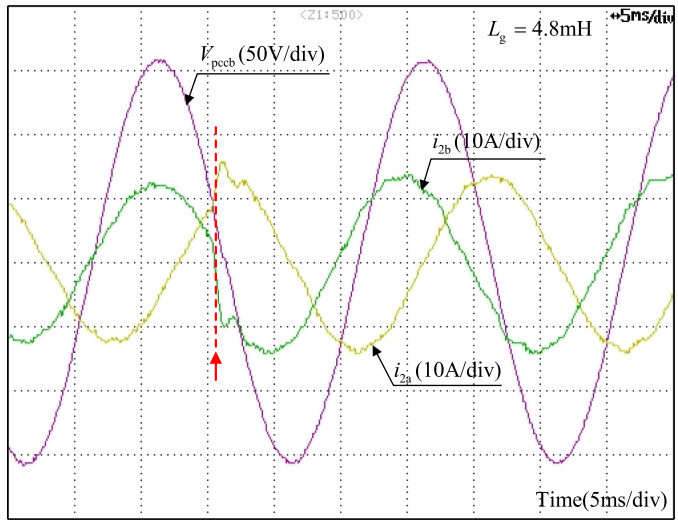

Fig. 14. Measured grid-injected currents under the condition of sharp current phase variation when $L_g = 4.8$ mH.

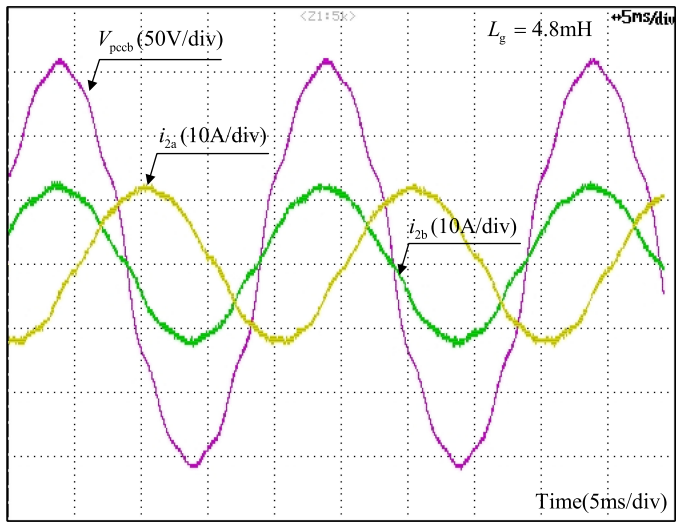

Fig. 15. Measured grid-injected currents under voltage distortion under $L_g = 4.8$ mH.

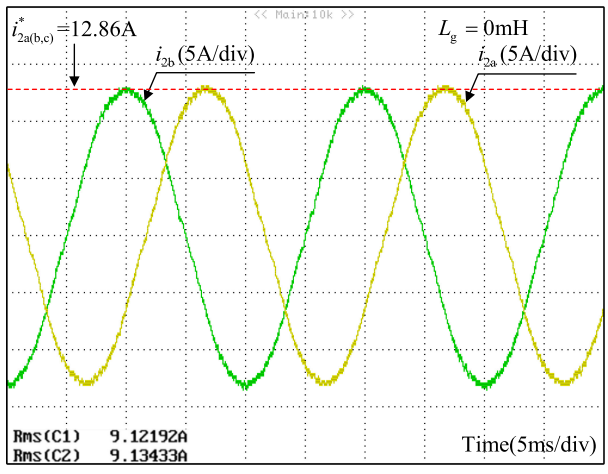

Fig. 16. Grid-injected current with zero steady-state error with $L_g = 0$ mH.

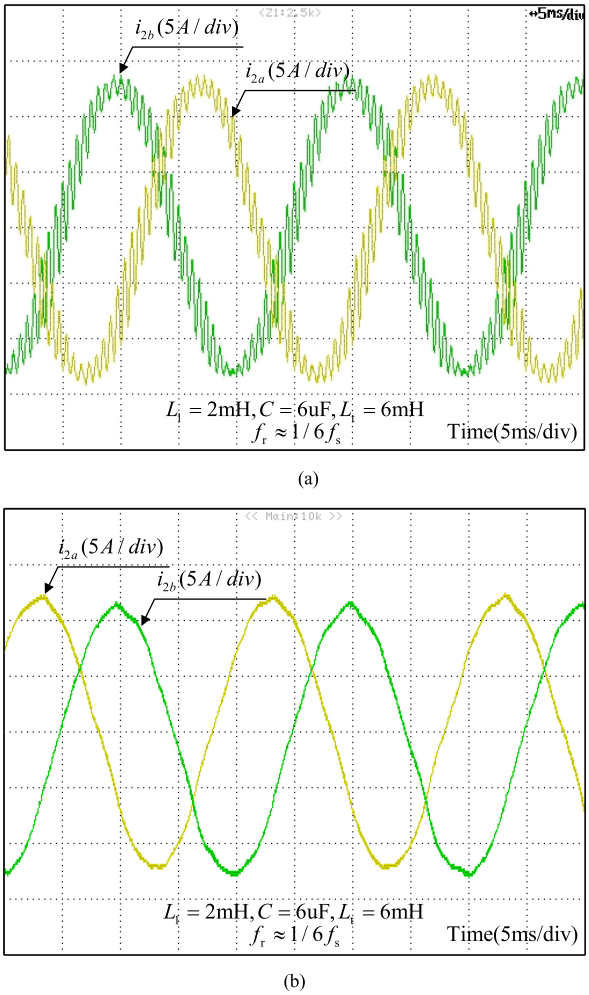

Fig. 17. Measured grid-injected current under $f_r \approx f_s/6$. (a) Conventional CCF control method. (b) Proposed PBC control method.

proposed PBC controller has a strong ability to resist the adverse effect caused by the harmonic grid voltage.

Fig. 16 shows the measured grid-injected current when the PI regulator is instead of r_1, i.e., the method to achieve zero steady-state error of grid-injected current. It can be seen that the rms value is about 9.1 A (the reference rms value is 9.09 A), which means the zero steady-state error can be also easily realized for the proposed PBC.

As analyzed above, the PBC controller can keep stable even if the resonant frequency equals 1/6 of the sampling frequency, while the conventional PR with CCF control method cannot. With $L_1 = 2$ mH, $C = 6$ μF and $L_t = 6$ mH, the characteristic resonant frequency of the system is calculated as 1678 Hz $\approx$ 1667 Hz ($1/6 f_s$), and the grid-injected current under this situation using the conventional CCF method and proposed PBC method is shown in Fig. 17. It can be seen from Fig. 17(b) that the grid-injected current is stable without any oscillation when the proposed PBC controller is adopted, while the grid-injected current is serious oscillation with conventional CCF method as shown in Fig. 17(a). Therefore, compared with the conventional

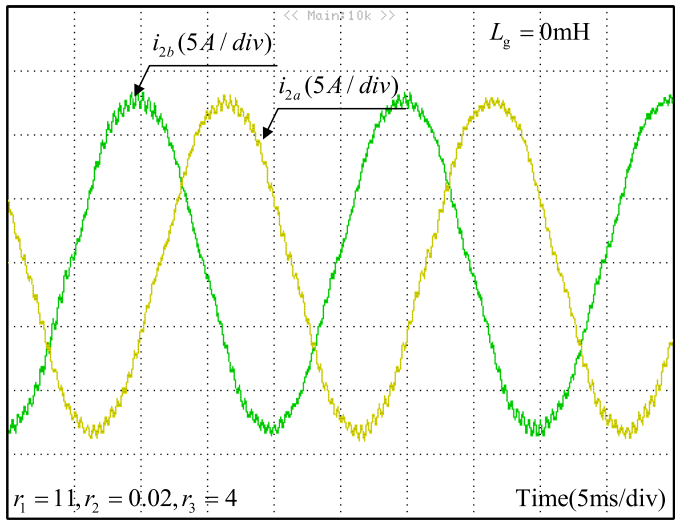

Fig. 18. Grid-injected current with $r_1 = 11$, $r_2 = 0.02$, $r_3 = 4$ when $L_g = 0$ mH.

CCF method, the proposed PBC controller has the higher robustness against parameters drift.

Fig. 18 shows the grid-injected current with $r_1 = 11, r_2 = 0.02$, $r_3 = 4$ when $L_g = 0$ mH. It can be seen that the grid-injected currents appear oscillation, when the value of r_1 higher than the calculated upper boundary of 10.1. Note that due to the actual resistance in the experimental device, the critical value of r_1 to trigger off the oscillation is a little bigger than the theoretical calculation.

VI. Conclusion

In this article, we have analyzed why it is difficult to design the three damping gains in the PBC controller for the three-phase *LCL*-filtered GTI, and then put forward a step-by-step control parameters design strategy. The overall conclusion can be summarized as follows.

1) Based on the expectation of the minimized inherent steady-state error of grid-injected current, the three damping gains in the PBC controller for the *LCL*-filtered GTI can be effectively designed by using the proposed strategy, which provides a useful guideline for engineers.
2) The designed PBC controller can maintain the system stable, even when parameters of *LCL* filter vary in the range from –33% to +33% and the grid impedance varies in the range from 0% to +400% of L_2. Compared with the conventional CCF AD control method for *LCL*-filtered GTI, the proposed PBC controller can achieve higher robustness against the parameter drifts of *LCL* filter and grid impedance.
3) State observer technology can be successfully applied in the proposed PBC controller, resulting in the saved sensors as well as costs.

The effectiveness of the proposed PBC controller has been fully verified via a 3 kW/3-phase/110 V experimental lab setup based on dSPACE DS1202.

APPENDIX

The expressions of *A, B, C,* and *D*

$$\begin{aligned}A = {} & (s^3C_eL_{1e}L_{2e} + s^2r_1C_eL_{1e} + s^2r_2L_{1e}L_{2e} + s^2r_3C_eL_{2e} \\ & + s^2C_eR_{1e}L_{2e} + s^2C_eL_{1e}R_{2e} + sr_1C_eR_{1e} + sr_2R_{1e}L_{2e} \\ & + sr_2L_{1e}R_{2e} + sr_3C_eR_{2e} + sr_1r_2L_{1e} + sr_2r_3L_{2e} \\ & + sr_1r_3C_e + sC_eR_{1e}R_{2e} - 3s\omega^2L_{1e}C_eL_{2e} + sL_{1e} \\ & + sL_{2e} + r_1r_2R_{1e} + r_2R_{1e}R_{2e} + r_2r_3R_{2e} \\ & - \omega^2L_{1e}C_eR_{2e} - \omega^2r_1L_{1e}C_e - \omega^2r_2L_{1e}L_{2e} \\ & - \omega^2r_3C_eL_{2e} - \omega^2C_eR_{1e}L_{2e} + r_1r_2r_3 + r_1 + r_3 \\ & + R_{1e} + R_{2e})e^{-1.5sT_s} \\ B = {} & (3s^2\omega L_{1e}C_eL_{2e} + 2s\omega r_1L_{1e}C_e + 2s\omega r_2L_{1e}L_{2e} \\ & + 2s\omega r_3C_eL_{2e} + 2s\omega C_eR_{1e}L_{2e} + 2s\omega L_{1e}C_eR_{2e} \\ & + \omega r_1C_eR_{1e} + \omega r_2L_{1e}R_{2e} + \omega r_2R_{1e}L_{2e} + \omega r_3C_eR_{2e} \\ & + \omega r_1r_2L_{1e} + \omega r_2r_3L_{2e} + \omega r_1r_3C_e + \omega C_eR_{1e}R_{2e} \\ & - \omega^3L_{1e}C_eL_{2e} + \omega L_{1e} + \omega L_{2e})e^{-1.5sT_s} \\ C = {} & (2s\omega r_1L_{1e}C_e + 2s\omega r_2L_{1e}L_2 + 2s\omega r_3CL_2 + \omega r_1C_eR_{1e} \\ & + \omega r_2L_{1e}R_2 + \omega r_2R_{1e}L_2 + \omega r_3CR_2 + \omega r_1r_2L_{1e} \\ & + \omega r_2r_3L_2 + \omega r_1r_3C_e)e^{-1.5sT_s} + (3s^2\omega L_1CL_2 \\ & + 2s\omega CR_1L_2 + 2s\omega L_1CR_2 - \omega^3L_1CL_2 + \omega CR_1R_2 \\ & + \omega L_1 + \omega L_2) \\ D = {} & (s^3CL_1L_2 + s^2CR_1L_2 + s^2CL_1R_2 + sCR_1R_2 \\ & - 3s\omega^2L_1CL_2 + sL_1 + sL_2 + R_1 + R_2 - \omega^2CR_1L_2 \\ & - \omega^2L_1CR_2) + (s^2r_1C_eL_{1e} + s^2r_2L_{1e}L_2 + s^2r_3CL_2 \\ & + sr_1C_eR_{1e} + sr_2R_{1e}L_2 + sr_2L_{1e}R_2 + sr_3CR_2 \\ & + sr_1r_2L_{1e} + sr_2r_3L_2 + sr_1r_3C_e + r_1r_2R_{1e} \\ & + r_2R_{1e}R_2 + r_2r_3R_2 - \omega^2r_1L_{1e}C_e - \omega^2r_2L_{1e}L_2 \\ & - \omega^2r_3CL_2 + r_1r_2r_3 + r_1 + r_3)e^{-1.5sT_s}.\end{aligned}$$

REFERENCES

[1] F. Blaabjerg, R. Teodorescu, M. Liserre, and A. V. Timbus, "Overview of control and grid synchronization for distributed power generation systems," *IEEE Trans. Ind. Electron.*, vol. 53, no. 5, pp. 1398–1409, Oct. 2006.

[2] W. Wu, Y. He, and F. Blaabjerg, "An *LLCL* power filter for single- phase grid-tied inverter," *IEEE Trans. Power Electron.*, vol. 27, no. 2, pp. 782–789, Feb. 2012.

[3] W. Wu, Y. Liu, Y. He, H. S. Chung, M. Liserre, and F. Blaabjerg, "Damping methods for resonances caused by LCL-filter-based current-controlled grid-tied power inverters: An overview," *IEEE Trans. Ind. Electron.*, vol. 64, no. 9, pp. 7402–7413, Sep. 2017.

[4] R. Peña-Alzola, M. Liserre, F. Blaabjerg, R. Sebastián, J. Dannehl, and F. W. Fuchs, "Analysis of the passive damping losses in LCL-filter-based grid converters," *IEEE Trans. Power Electron.*, vol. 28, no. 6, pp. 2642–2646, Jun. 2013.

[5] A. Kouchaki and M. Nymand, "Analytical design of passive LCL filter for three-phase two-level power factor correction rectifiers," *IEEE Trans. Power Electron.*, vol. 33, no. 4, pp. 3012–3022, Apr. 2018.

[6] W. Wu, Y. He, T. Tang, and F. Blaabjerg, "A new design method for the passive damped LCL and LLCL filter-based single-phase grid-tied inverter," *IEEE Trans. Ind. Electron.*, vol. 60, no. 10, pp. 4339–4350, Oct. 2013.

[7] D. Pan, X. Ruan, C. Bao, W. Li, and X. Wang, "Capacitor-current-feedback active damping with reduced computation delay for improving robustness of LCL-type grid-connected inverter," *IEEE Trans. Power Electron.*, vol. 29, no. 7, pp. 3414–3427, Jul. 2014.

[8] Y. He, X. Wang, X. Ruan, D. Pan, X. Xu, and F. Liu, "Capacitor-current proportional-integral positive feedback active damping for LCL-type grid-connected inverter to achieve high robustness against grid impedance variation," *IEEE Trans. Power Electron.*, vol. 34, no. 12, pp. 12423–12436, Dec. 2019.

[9] L. Jia, X. Ruan, W. Zhao, Z. Lin, and X. Wang, "An adaptive active damper for improving the stability of grid-connected inverters under weak grid," *IEEE Trans. Power Electron.*, vol. 33, no. 11, pp. 9561–9574, Nov. 2018.

[10] W. Yao, Y. Yang, X. Zhang, F. Blaabjerg, and P. C. Loh, "Design and analysis of robust active damping for LCL filters using digital notch filters," *IEEE Trans. Power Electron.*, vol. 32, no. 3, pp. 2360–2375, Mar. 2017.

[11] M. Ben Saïd-Romdhane, M. W. Naouar, I. Slama-Belkhodja, and E. Monmasson, "Robust active damping methods for LCL filter-based grid-connected converters," *IEEE Trans. Power Electron.*, vol. 32, no. 9, pp. 6739–6750, Sep. 2017.

[12] Y. Liu, W. Wu, Y. He, Z. Lin, F. Blaabjerg, and H. S. H. Chung, "An efficient and robust hybrid damper for LCL- or LLCL-based grid-tied inverter with strong grid-side harmonic voltage effect rejection," *IEEE Trans. Ind. Electron.*, vol. 63, no. 2, pp. 926–936, Feb. 2016.

[13] Y. Lei, W. Xu, C. Mu, Z. Zhao, H. Li, and Z. Li, "New hybrid damping strategy for grid-connected photovoltaic inverter with LCL filter," *IEEE Trans. Appl. Supercond.*, vol. 24, no. 5, pp. 1–8, Oct. 2014.

[14] J. Ye, A. Shen, Z. Zhang, J. Xu, and F. Wu, "Systematic design of the hybrid damping method for three-phase inverters with high-order filters," *IEEE Trans. Power Electron.*, vol. 33, no. 6, pp. 4944–4956, Jun. 2018.

[15] D. Pan, X. Ruan, C. Bao, W. Li, and X. Wang, "Optimized controller design for LCL-type grid-connected inverter to achieve high robustness against grid-impedance variation," *IEEE Trans. Ind. Electron.*, vol. 62, no. 3, pp. 1537–1547, Mar. 2015.

[16] M. Cespedes and J. Sun, "Adaptive control of grid-connected inverters based on online grid impedance measurements," *IEEE Trans. Sustain. Energy*, vol. 5, no. 2, pp. 516–523, Apr. 2014.

[17] J. Liu, W. Wu, H. S. Chung, and F. Blaabjerg, "Disturbance observer-based adaptive current control with self-learning ability to improve the grid-injected current for LCL -filtered grid-connected inverter," *IEEE Access*, vol. 7, pp. 105376–105390, 2019.

[18] Z. Zou, G. Buticchi, and M. Liserre, "Grid identification and adaptive voltage control in a smart transformer-fed grid," *IEEE Trans. Power Electron.*, vol. 34, no. 3, pp. 2327–2338, Mar. 2019.

[19] M. Merai, W. Naouar, I. Slama-Belkhodja, and E. Monmasson, "An adaptive PI controller design for DC-link voltage control of single-phase grid-connected converters," *IEEE Trans. Ind. Electron.*, vol. 66, no. 8, pp. 6241–6249, Aug. 2019.

[20] D. Martin and E. Santi, "Autotuning of digital deadbeat current controllers for grid-tie inverters using wide bandwidth impedance identification," *IEEE Trans. Ind. Appl.*, vol. 50, no. 1, pp. 441–451, Jan./Feb. 2014.

[21] Y. He, H. S. Chung, C. N. Ho, and W. Wu, "Modified cascaded boundary-deadbeat control for a virtually-grounded three-phase grid-connected inverter with LCL filter," *IEEE Trans. Power Electron.*, vol. 32, no. 10, pp. 8163–8180, Oct. 2017.

[22] X. Xing, C. Zhang, A. Chen, H. Geng, and C. Qin, "Deadbeat control strategy for circulating current suppression in multiparalleled three-level inverters," *IEEE Trans. Ind. Electron.*, vol. 65, no. 8, pp. 6239–6249, Aug. 2018.

[23] S. R. Mohapatra and V. Agarwal, "Model predictive controller with reduced complexity for grid-tied multilevel inverters," *IEEE Trans. Ind. Electron.*, vol. 66, no. 11, pp. 8851–8855, Nov. 2019.

[24] N. Panten, N. Hoffmann, and F. W. Fuchs, "Finite control set model predictive current control for grid-connected voltage-source converters with LCL filters: A study based on different state feedbacks," *IEEE Trans. Power Electron.*, vol. 31, no. 7, pp. 5189–5200, Jul. 2016.

[25] Y. Shan, J. Hu, and J. M. Guerrero, "A model predictive power control method for PV and energy storage systems with voltage support capability," *IEEE Trans. Smart Grid*, to be published.

[26] J. Scoltock, T. Geyer, and U. K. Madawala, "Model predictive direct power control for grid-connected NPC converters," *IEEE Trans. Ind. Electron.*, vol. 62, no. 9, pp. 5319–5328, Sep. 2015.

[27] X. Hao, X. Yang, T. Liu, L. Huang, and W. Chen, "A sliding-mode controller with multiresonant sliding surface for single-phase grid-connected VSI with an LCL filter," *IEEE Trans. Power Electron.*, vol. 28, no. 5, pp. 2259–2268, May 2013.
[28] R. P. Vieira, L. T. Martins, J. R. Massing, and M. Stefanello, "Sliding mode controller in a multiloop framework for a grid-connected VSI with LCL filter," *IEEE Trans. Ind. Electron.*, vol. 65, no. 6, pp. 4714–4723, Jun. 2018.
[29] L. T. Martins, M. Stefanello, H. Pinheiro, and R. P. Vieira, "Current control of grid-tied LCL-VSI with a sliding mode controller in a multiloop approach," *IEEE Trans. Power Electron.*, vol. 34, no. 12, pp. 12356–12367, Dec. 2019.
[30] M. M. Namazi, S. M. S. Nejad, A. Tabesh, A. Rashidi, and M. Liserre, "Passivity-based control of switched reluctance-based wind system supplying constant power load," *IEEE Trans. Ind. Electron.*, vol. 65, no. 12, pp. 9550–9560, Dec. 2018.
[31] J. Min, F. Ma, Q. Xu, Z. He, A. Luo, and A. Spina, "Analysis, design, and implementation of passivity-based control for multilevel railway power conditioner," *IEEE Trans. Ind. Informat.*, vol. 14, no. 2, pp. 415–425, Feb. 2018.
[32] Z. Liu, Z. Geng, and X. Hu, "An approach to suppress low frequency oscillation in the traction network of high-speed railway using passivity-based control," *IEEE Trans. Power Syst.*, vol. 33, no. 4, pp. 3909–3918, Jul. 2018.
[33] Y. Lei, X. Lin, and Y. Zhu, "Passivity-Based control strategy for SMES under an unbalanced voltage condition," *IEEE Access*, vol. 6, pp. 28768–28776, 2018.
[34] J. Li, X. Lv, B. Zhao, Y. Zhang, Q. Zhang, and J. Wang, "Research on passivity based control strategy of power conversion system used in the energy storage system," *IET Power Electron*., vol. 12, no. 3, pp. 392–399, Mar. 2019.
[35] T.-S. Lee, "Lagrangian modeling and passivity-based control of three-phase AC/DC voltage-source converters," *IEEE Trans. Ind. Electron.*, vol. 51, no. 4, pp. 892–902, Aug. 2004.
[36] Y. Gui, B. Wei, M. Li, J. M. Guerrero, and J. C. Vasquez, "Passivity-based coordinated control for islanded AC microgrid," *Appl. Energy*, vol. 229, pp. 551–561, 2018.
[37] Y. Chen, M. Wen, E. Lei, X. Yin, J. Lai, and Z. Wang, "Passivity-based control of cascaded multilevel converter based D-STATCOM integrated with distribution transformer," *Elect. Power Syst. Res.*, vol. 154, pp. 1–12, Jan. 2018.
[38] J. Lai, Y. Xin, L. Jiang, X. Yin, Z. Wang, and Z. Ullah, "Disturbance observer based PBC for static synchronous compensator under system disturbances," *IEEE Trans. Power Electron*, vol. 34, no. 11, pp. 11467–11481, Nov. 2019.
[39] X. Mu, J. Wang, W. Wu, and F. Blaabjerg, "A modified multifrequency passivity-based control for shunt active power filter with model-parameter-adaptive capability," *IEEE Trans. Ind. Electron.*, vol. 65, no. 1, pp. 760–769, Jan. 2018.
[40] H. Komurcugil, "Improved passivity-based control method and its robustness analysis for single-phase uninterruptible power supply inverters," *IET Power Electron*., vol. 8, no. 8, pp. 1558–1570, Aug. 2015.
[41] J. Wang, X. Mu, and Q. K. Li, "Study of passivity-based decoupling control of T-NPC PV grid-connected inverter," *IEEE Trans. Ind. Electron.*, vol. 64, no. 9, pp. 7542–7551, Sep. 2017.
[42] Y. Jiang, C. Qin, X. Xing, X. Li, and C. Zhang, "A hybrid passivity-based control strategy for three-level T-type inverter in LVRT operation," *IEEE J. Emerg. Sel. Topics Power Electron.*, to be published.
[43] J. Lai, X. Yin, E. Lei, Y. Chen, and X. Yin, "Passivity control based on Euler-Lagrangian model for D-STATCOM with LCL filter," in *Proc.12th World Congr. Intell. Control Autom.*, Guilin, China, 2016, pp. 1561–1565.
[44] J. Lai *et al.*, "System modeling and cascaded passivity based control for distribution transformer integrated with static synchronous compensator," *Int. J. Elect. Power Energy Syst.*, vol. 113, pp. 1035–1046, 2019.
[45] R. Ortega, A. Loria, P. J. Nicklasson, and H. Sira-Ramirez, *Passivity-Based Control of Euler–Lagrange Systems*. Berlin, Germany: Springer-Verlag, 1998.
[46] J. Kukkola and M. Hinkkanen, "Observer-based state-space current control for a three-phase grid-connected converter equipped with an LCL filter," *IEEE Trans. Ind. Appl.*, vol. 50, no. 4, pp. 2700–2709, Jul./Aug. 2014.
[47] V. Miskovic, V. Blasko, T. M. Jahns, A. H. C. Smith, and C. Romenesko, "Observer-based active damping of LCL resonance in grid-connected voltage source converters," *IEEE Trans. Ind. Appl.*, vol. 50, no. 6, pp. 3977–3985, Nov./Dec. 2014.
[48] Z. Zhang *et al.*, "Principle and robust impedance-based design of grid-tied inverter with LLCL-filter under wide variation of grid-reactance," *IEEE Trans. Power Electron.*, vol. 34, no. 5, pp. 4362–4374, May 2019.
[49] R. B. Ridley, B. H. Cho, and F. C. Y. Lee, "Analysis and interpretation of loop gains of multiloop-controlled switching regulators (power supply circuits)," *IEEE Trans. Power Electron.*, vol. 3, no. 4, pp. 489–498, Oct. 1988.
[50] D. Sivadas and K. Vasudevan, "Stability analysis of three-loop control for three-phase voltage source inverter interfaced to the grid based on state variable estimation," *IEEE Trans. Ind. Appl.*, vol. 54, no. 6, pp. 6508–6518, Nov./Dec. 2018.

Jinping Zhao was born in Shandong, China, in 1993. He received the B.S. degree in ship electrical and electronic engineering in 2017 from Shanghai Maritime University, Shanghai, China, where he is currently working toward the M.S. degree in electrical engineering.

His current research interests include nonlinear control, digital control techniques of power converters, and renewable energy generation system.

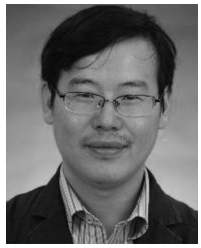

Weimin Wu (Member, IEEE) received the Ph.D. degree in electrical engineering from the College of Electrical Engineering, Zhejiang University, Hangzhou, China, in 2005.

He worked as a Research Engineer with the Delta Power Electronic Center (DPEC), Shanghai, from July 2005 to June 2006. Since July 2006, he has been a Faculty Member with Shanghai Maritime University, Shanghai, where he is currently a Full Professor with the Department of Electrical Engineering. He was a Visiting Professor with the Center for Power Electronics Systems (CPES), Virginia Polytechnic Institute and State University, Blacksburg, USA, from September 2008 to March 2009. From November 2011 to January 2014, he was also a Visiting Professor with the Department of Energy Technology, Aalborg University, Demark, working at the Center of Reliable Power Electronics (CORPE). He has coauthored more than 100 papers and holds eight patents. His research interests include power converters for renewable energy systems, power quality, smart grid, and energy storage technology.

Dr. Wu serves as an Associate Editor for the IEEE TRANSACTIONS ON INDUSTRY ELECTRONICS.

Zhikang Shuai (Senior Member, IEEE) received the B.S. and Ph.D. degrees in electrical engineering from the College of Electrical and Information Engineering, Hunan University, Changsha, China, in 2005 and 2011, respectively.

He was at Hunan University, as an Assistant Professor between 2009 and 2012, an Associate Professor in 2013, and a Professor in 2014. His research interests include power quality control, power electronics, and microgrid stability analysis and control.

Dr. Shuai is the Associate Editor of IEEE JOURNAL OF EMERGING AND SELECTED TOPICS IN POWER ELECTRONICS, *CSEE Journal of Power and Energy Systems*, and *Chinese Journal of Electrical Engineering*. He was the recipient of the 2010 National Scientific and Technological Awards of China, the 2012 Hunan Technological Invention Awards of China, and the 2007 Scientific and Technological Awards from the National Mechanical Industry Association of China.

An Luo (Senior Member, IEEE) was born in Changsha, China, in 1957. He received the B.S. and M.S. degrees in industrial automation from Hunan University, Changsha, in 1982 and 1986, respectively, and the Ph.D. degree in fluid power transmission and control from Zhejiang University, Hangzhou, China, in 1993. Between 1996 and 2002, he was a Professor with Central South University. Since 2003, he has been a Professor with the College of Electrical and Information Engineering, Hunan University, where he also serves as the Chief of National Electric Power Conversion and Control Engineering Technology Research Center. His research interests mainly include distributed generation, microgrid, and power quality.

Dr. Luo was elected to the Chinese National Academy of Engineering in 2015, the highest honor for scientists and engineers and scientists in China. He has won the highly prestigious China National Science and Technology Awards three times (2014, 2010, and 2006).

Henry Shu-Hung Chung (Fellow, IEEE) received the B.Eng. and Ph.D. degrees in electrical engineering from the Hong Kong Polytechnic University, Hong Kong, in 1991 and 1994, respectively.

Since 1995, he has been with the City University of Hong Kong, Hong Kong, where he is currently a Chair Professor with the Department of Electrical Engineering and the Director of the Center for Smart Energy Conversion and Utilization Research. His current research interests include renewable energy conversion technologies, lighting technologies, smart grid technologies, and computational intelligence for power electronic systems. He has edited one book, authored eight research book chapters, and more than 460 technical papers including 200 refereed journal papers in his research areas, and holds 50 patents.

Dr. Chung was the Chair of the Technical Committee of the High-Performance and Emerging Technologies, IEEE Power Electronics Society in 2010–2014. He is currently an Associate Editor of the IEEE TRANSACTIONS ON POWER ELECTRONICS and IEEE JOURNAL OF EMERGING AND SELECTED TOPICS IN POWER ELECTRONICS. He was the Editor-in-Chief of the IEEE POWER ELECTRONICS LETTERS in 2014–2018. He has received numerous industrial awards for his invented energy saving technologies.

Frede Blaabjerg (Fellow, IEEE) received the Ph.D. degree in electrical engineering from Aalborg University, Aalborg, Denmark, in 1992.

He was with ABB-Scandia, Randers, Denmark, from 1987 to 1988. He became an Assistant Professor in 1992, an Associate Professor in 1996, and a Full Professor of power electronics and drives in 1998. In 2017 he became a Villum Investigator. His current research interests include power electronics and its applications such as in wind turbines, photovoltaic systems, reliability, harmonics, and adjustable speed drives. He has published more than 450 journal papers in the fields of power electronics and its applications. He is the co-author of two monographs and editor of six books in power electronics and its applications.

Dr. Blaabjerg was the Editor-in-Chief of the IEEE TRANSACTIONS ON POWER ELECTRONICS from 2006 to 2012.